Article:
Wright, TJ (2016) The earthquake deformation cycle. Astronomy and Geophysics, 54 (7). 4.20-4.26. ISSN: 1366-8781

https://doi.org/10.1093/astrogeo/atw148

The Earthquake Deformation Cycle and Seismic Hazard in the Continents

The 2015 Bullerwell Lecture

Tim J Wright

COMET, School of Earth and Environment, University of Leeds, UK

Abstract/Intro Paragraph.

Earthquakes seem impossible to predict, yet they are associated with the slow deformation of tectonic plates. In the 2015 Bullerwell lecture, Tim Wright reviews observations of time-dependent surface deformation in fault zones, and uses these observations to place constraints on feasible models of the earthquake deformation cycle. The results have implications for the mechanics of fault zones and the strength of the continental lithosphere, and are critical if we are to use short-term geodetic observations as tool for assessing seismic hazard.

Mailing addresses: Tim Wright, (t.j.wright@leeds.ac.uk);

Table of Contents

1. Introduction

On 26 December 2003, nearly half the population of the town of Bam (Iran) was killed in 10 seconds of shaking. On 12 January 2010, more than 200 thousand lives and a year's GDP were lost in Haiti in a devastating Magnitude 7 earthquake[1]. On 25 April 2015, nearly 10,000 people were killed across huge swathes of Nepal when the Himalayan Frontal Thrust slipped by 8 m (Elliott, 2016). The catalogue of earthquake disasters in the first 15 years of the 21st century now contains eight individual events that have each resulted in the loss of ~10,000 lives or more (Table 1). Six of these occurred in the continental interiors, many on faults that were unknown prior to the earthquake, or whose hazard had been underestimated.

Assessing seismic hazard in the continents is difficult and existing hazard assessment methods often fail, particularly in areas with relatively few earthquakes. I will argue that we can do better by using new and rapidly improving measurements of how the continents deform. But earthquakes typically occur every few hundred to few thousand years on any individual fault, and our observations of deformation usually only cover time periods of a decade or less. To use these short-term observations of deformation in seismic hazard, we need better models of how fault zones deform in space and time. I will describe the key observations that any successful model must be able to reproduce, and use these to test competing models. The results have implications for the deep structure of fault zones and the strength of continental lithosphere.

[1] http://www.emdat.be/ database accessed 28 October 2015

Table 1 – Mass-casualty earthquakes in 20th century. Data from USGS[2]. Those coloured red occurred in the continents

Year	Earthquake	Lives Lost
2001	Bhuj	20,000
2003	Bam	31,000
2004	Sumatra	228,000
2005	Pakistan	86,000
2008	Sichuan	88,000
2010	Haiti	326,000
2011	Tohoku	21,000
2015	Nepal	9000+

[2] http://earthquake.usgs.gov/earthquakes/world/world_deaths.php accessed 8 December 2016. Note that others estimate fewer than 100,000 deaths in the Haiti earthquake. The number of casualties in the 2015 Nepal earthquake has yet to be officially confirmed

2. Seismic hazard in the continents

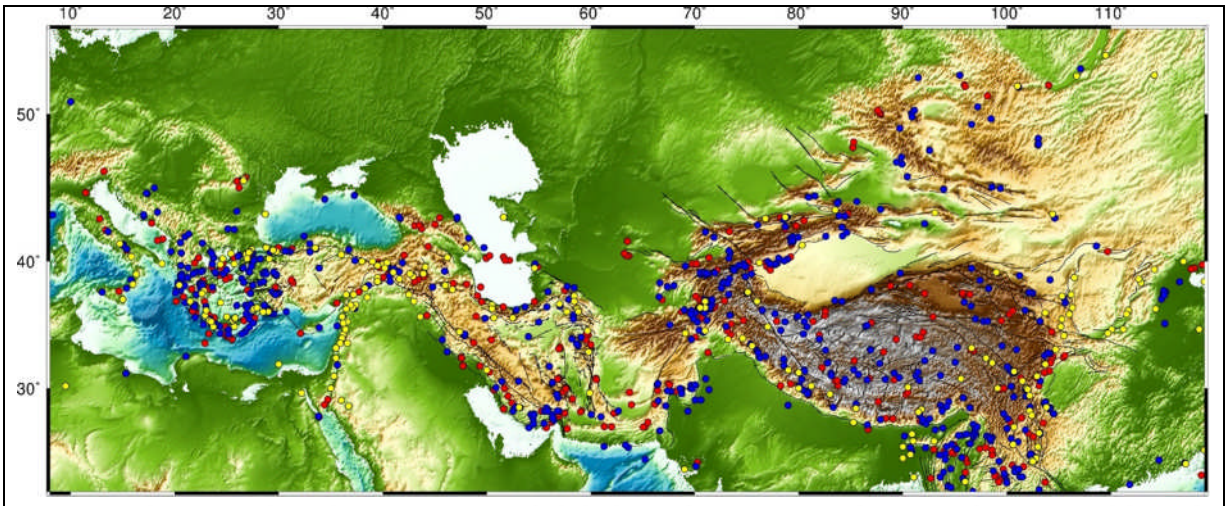

Figure 1: Distribution of earthquakes in the continents. Background colours show the topography from the Shuttle Radar Topography Mission. Each circle is an earthquake with M>=6, with its colour denoting it time of occurrence and source catalogue.

Estimating seismic hazard in the continents is notoriously difficult. There are three main reasons for this. Firstly, plate boundary deformation zones in the continents are wide. For example, the collision of the Indian plate with Eurasia has created a zone of thickened crust and high seismicity that stretches for up to 2000 km from the foothills of the Himalayas to the distant steppes of Mongolia (Figure 1). We are not just dealing with the hazard from a single, narrow plate-boundary fault, as we might be when we are looking at the subduction zones that circle the Pacific. In continental deformation zones, we are dealing with vast networks of faults on all scales.

Secondly, earthquakes on any individual fault are rare and so earthquake catalogues are only partial records. We can see this very clearly by comparing catalogues covering different time periods (Figure 1). For example, in Northern Italy, M6.5 and M6.0 earthquakes occurred in Friuli and Emilia in 1976 and 2012 in locations that lack any historical records of past seismicity. In contrast, the Dead Sea Fault in the Middle East, and Ordos block in China have suffered devastating earthquakes in the past, but have been seismically quiet in the past 100 years. Maps of active faults and palaeoseismological investigations enable us to look back even further in time; many of the active faults marked on Figure 1, for example in Central Asia, have no records of previous earthquakes, yet they were clearly created by major earthquakes.

Finally, although we have made enormous advances in our ability to read the landscape for signs of tectonic activity (e.g. Jackson, 2001), we still don't know where all the active faults are. While further painstaking work scouring satellite imagery and checking sites in the field can and will improve our knowledge of active faults (e.g. Walker et al., 2015), many faults will only be discovered when they fail in earthquakes. For example, the faults that caused the M6.5 Bam (Iran) and M7.0 Darfield (New Zealand) earthquakes could not have been identified before they failed: Both occurred on strike slip faults in areas of active sedimentation and did not create any long-term signature in the landscape.

A brief comparison with volcanic hazard illustrates the challenges that we face when trying reduce human and monetary losses from earthquakes in the continents. There are 1390 subaerial volcanoes that listed by the Global Volcano Database as having been active in the last ~10,000 years (Siebert and Simkin, 2014). We know where they all are. Furthermore, most volcanoes are isolated point sources of hazard, and, even close to volcanoes, the relative safety of different areas can be readily assessed. Finally, almost all volcanic eruptions are preceded

by precursory activity, enabling people to issue warnings and evacuate, at least if the volcano is well monitored. By contrast, earthquakes occur on faults that have not all been identified, they are extended sources, and they usually occur with no warning. Given this, perhaps it is not a surprise, although it is very sobering, that more people have died in the first 15 years of the 21st century (Table 1) than in all volcanic eruptions in recorded history (Witham, 2005).

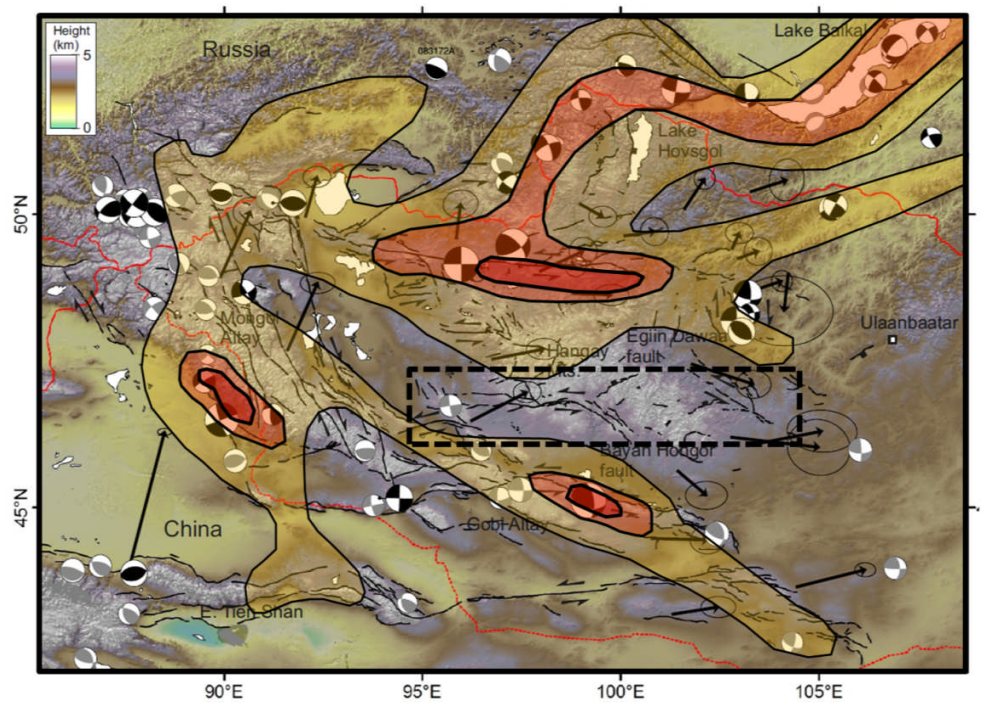

Figure 2: Active Faulting, Seismicity and Seismic Hazard in Mongolia. Active Faults (black lines), Seismicity (black/grey focal spheres) and GPS velocities (black arrows) are from Walker et al. (2015) and references therein. The yellow, pink and red shaded regions show areas where there is a 20% chance in a 50 year period of exceeding intensities of degree VII,

VIII, and IX+ respectively on the Modified Mercalli Scale in the UN's 2010 seismic hazard map for Mongolia[3]. Note the active faults within the dashed black box, which lie within a region of low seismic hazard.

Despite the challenges, assessing seismic hazard is an important endeavour. For the last few decades, the standard method has been Probabilistic Seismic Hazard Assessment (PSHA; Reiter, 1991). This method uses catalogues of past earthquakes, estimates of recurrence rates, and information from active fault maps, if available, to identify all possible earthquakes in a region. For any point on the Earth, the amount of shaking from all these seismic sources is then calculated, using equations that use local conditions, such as whether you are on bedrock or soft sediment, to predict the ground motion based on distance to the source and its strength. The earthquake catalogues are used to estimate how often earthquakes of different magnitudes occur in each location. By combining this information, a probability of experiencing strong shaking (acceleration) during a certain time interval can be calculated. Probabilistic Seismic Hazard Assessment has been incredibly successful and is widely applied; building codes across the world mandate construction to withstand the likely shaking, and, where these are rigorously enforced (Ambraseys and Bilham, 2011), countless lives have undoubtedly been saved.

The hazard models produced by PSHA are, however, only as good as the input data. In areas with relatively low rates of damaging seismicity, we have seen that even historical catalogues fail to capture all the potential earthquakes that might occur (Figure 1). In these areas, models of future seismic hazard that are based on the distribution of where earthquakes

[3] http://www.preventionweb.net/english/professional/maps/v.php?id=15692 Accessed 8 January 2016

have occurred in the past can be poor at predicting where earthquakes might occur in the future. This was devastatingly illustrated by the Haiti earthquake, which occurred in an area where the best available PSHA hazard model before the earthquake placed the capital, Port-au-Prince, in an area of relatively low seismic hazard (Stein et al., 2012). We can also see the problem very clearly in Mongolia, where the most recent seismic hazard map shows the highest potential for shaking in the three areas where large earthquakes have occurred in the past 100 years, despite the abundant evidence for equally hazardous active faults outside these areas (Figure 2). In fact, it could be argued that faults that have failed in the past in large earthquakes are less likely to fail in the future rather than more likely.

So, how can we do better? We could of course wait for all potential devastating earthquakes to occur, updating the hazard maps each time a new event occurs. But if we take this approach, our hazard maps won't be an accurate representation of the true hazard for thousands of years. Here I will argue that using measurements of how the ground deforms between earthquakes can provide an alternative. We have known for more than 100 years that earthquakes release strain energy that has built up in the intervals between earthquakes (Reid, 1910). If we accept the hypothesis that earthquakes only occur where strain energy has accumulated, we ought to be able to estimate future earthquake hazard by measuring the accumulation of strain between earthquakes. To achieve this requires us to be able to measure strain accumulation with sufficient accuracy [Box 1], and to develop models that can relate short-term observations of strain to the long-term activity of faults (Sections 3,4).

Box 1: Measuring deformation at fault zones with satellite geodesy.

Since the early 1990s, there has been a dramatic improvement in our ability to measure deformation around fault zones. Two technologies are particularly dominant in this field.

Neither technology was designed to achieve the accuracies that are required for measuring tectonic deformation, yet both are now being used to construct a complete picture of our deforming continents.

The first is technology uses data from Global Navigation Satellite Systems (GNSS) such as the US Global Positioning System (GPS). These systems were originally designed for military applications, but now have widespread civilian use, particularly in the navigation systems built into many cars and smartphones. GNSS satellites are essentially very accurate atomic clocks in orbit, constantly broadcasting a code containing their time and position. If we can see at least four of these satellites, and measure the time delay between transmission and receipt of the code, we can calculate our position anywhere on Earth. Information from 3 satellites is needed to obtain our 3D position; data from the fourth is required because our receivers on the ground don't use atomic clocks so we need to solve for the timing error. Using this method, the GNSS receiver in your phone/car will give you your position to an accuracy of about 5 m. This is clearly insufficient for measuring deformation at tectonic rates, which might be as slow as 1 mm/yr. To get around this problem, scientists realised that they could ignore the code and instead track the wave on which it is encoded. These carrier waves have a wavelength of about 20 cm, and we can track the phase of these signals (the position of the wave within the cycle) to an accuracy of about 2 mm as the satellites move along their orbits. By measuring these phase data from lots of satellites over time we can obtain absolute positions with an accuracy of about 1 mm. For good reviews of GNSS methodology see Misra and Enge (2006) and Blewitt (2007).

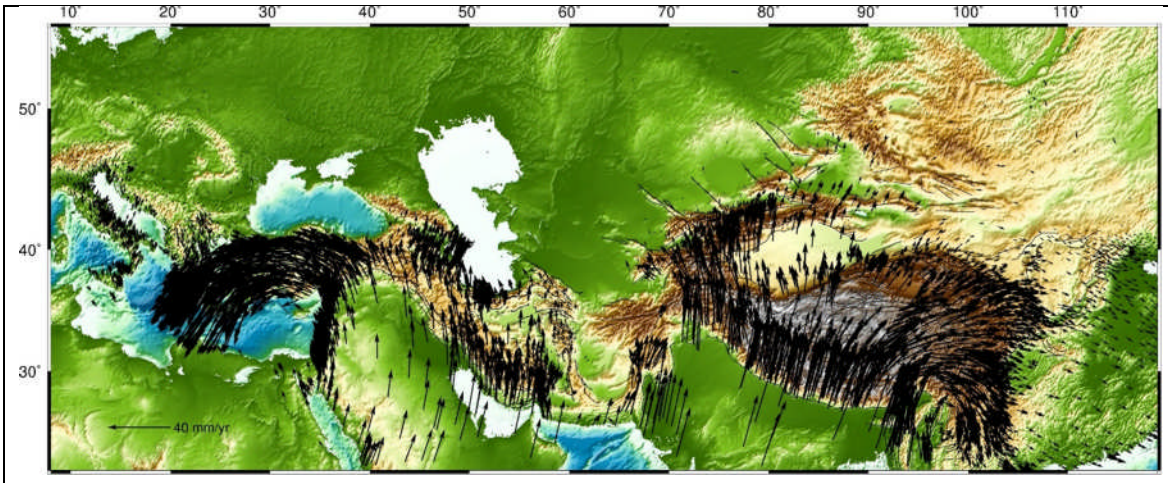

Figure 3: GNSS velocities in the Alpine Himalayan Belt, plotted relative to the Eurasian plate. Data compiled by Kreemer et al. (2014) for version 2 of the Global Strain Rate Model.

Place Figure 3 here, within box

Scientific GNSS receivers have been reduced in cost significantly over time. There are now many thousands of GNSS instruments installed permanently at sites across the planet, and more sites whose positions are measured in regular campaigns. All available GNSS data have recently been compiled and analysed by Corné Kreemer and colleagues at the University of Nevada, Reno, who have used the data to produce a global map of tectonic strain (Kreemer et al., 2014). Their latest model has is posted on a ~25 km grid and uses ~20,000 individual point velocities. This has improved greatly since their first model (Kreemer et al., 2003), which was constrained by only ~4000 velocities; data coverage will continue to improve in coming years as the community makes new and improved measurements. However, there are large gaps in the coverage in many tectonic areas, particularly in developing countries, which are not able to afford the installation and maintenance costs of dense permanent GNSS networks. Even in Japan and California, which have the densest GNSS coverages on Earth, stations spaced by 10-

50 km can be insufficient to distinguish between locked faults accumulating strain and those that creep steadily without building up strain.

A second satellite technology, Interferometric Synthetic Aperture Radar (InSAR), can make observations of surface motions with millimetric precision, a spatial resolution of a few tens of metres, and without instruments on the ground. Again, this technology was not designed for measuring tectonic deformation. Satellite radars were launched as an imaging technology, to provide images of the Earth for civilian and military applications. Unlike optical satellites, which passively record sunlight scattered from the Earth, and/or radiated heat, radar satellites actively transmit radar waves from the satellite, recording the backscattered energy at the satellite. Radar waves are electromagnetic radiation with a much longer wavelength (1 cm – 1 m) than visible light (0.4-0.7 μm), and these waves can see through clouds. Radar satellites provide an all-weather imaging tool, and with their own source of illumination they can acquire imagery at any time of day or night.

In the late 1980s, scientists at NASA's Jet Propulsion Laboratory realised that radar satellites can be used to measure surface movement (Goldstein and Zebker, 1987) by exploiting the fact that they emit a coherent source of waves – the radar waves are emitted at a known and consistent position within their wave cycle (phase). We can also measure the phase of the waves that return. The difference between these two values is a function of the distance between the satellite and the ground. However, with wavelengths of 2-20 cm typical for radar systems in use today, the radar waves travel a distance equivalent to several tens of millions of wavelengths on their round-trip journey to the Earth's surface. And we don't know the position of the satellite, and Earth's topography, well enough to know the nearest whole number of wavelengths along the radar beam's path. i.e. all we know is that the path length is equal to N

whole wavelengths, where *N* is an unknown integer, plus some fraction of a wavelength, which we can measure very precisely from the phase of the wave. Furthermore, the number of wavelengths, and hence the recorded phase, is also a function of the speed of propagation of the wave through the atmosphere and of any changes in phase that occur when the waves interact with the ground. Neither of these can be determined using independent data with sufficient precision to correct for their contributions to apparent changes in path length and phase.

We can solve these seemingly intractable problems using interferometry, by comparing the relative phase differences measured in two radar images acquired from approximately the same position in space, but at different times, and by comparing the phase values between two different positions on the ground within this phase difference image (interferogram). After making minor corrections for any changes in the satellite's position, and provided the ground surface hasn't changed significantly in the time between the two image acquisitions, the precise topography and the changes in phase that occur when the waves interact with the ground are nearly identical in the two images. These signals cancel out when forming the interferogram. Furthermore, if our knowledge of the satellite position is incorrect, this will affect all pixels in the image in a similar way, leading to only very long-wavelength contributions to the phase pattern in the interferogram. By examining relative phase chances between pixels in the interferogram, any changes in overall path length do not matter. Changes in atmospheric contributions will cause phase contributions, but the changes in atmospheric delay are much smaller than the total delay, and any changes are usually smooth in space. What we are left with then in the interferograms is primarily a function of the change in distance between the satellite and the ground. For a more technical review of how surface

displacements can be measured with InSAR, see Massonnet and Feigl (1998) and Burgmann et al. (2000).

InSAR was first used to measure the motion in earthquakes in the early 1990s (Massonnet et al., 1993), and by the early 2000s it was possible to combine multiple interferograms to measure tectonic strain (Wright et al., 2001, Peltzer et al., 2001). The methodologies have now become much more routine, and many key observations of the time-dependent deformation that occurs during the earthquake cycle have been made using InSAR (Wright et al., 2013). The launch of ESA's Sentinel-1A satellite in April 2014 boosted the observational capacity – images are now being acquired every 12 days for most of the tectonic and volcanic areas of the planet (Elliott, 2015).

The accuracy required of these geodetic techniques to be useful for seismic hazard assessment can be assessed in a number of ways. One is to compare geodetic strain rates, estimated from the global strain rate model, with a crude measure of the impact of earthquakes – the number of people who are killed because of earthquakes (Figure 4). This analysis shows that 96% of earthquake deaths occur in areas straining at rates higher than 10^{-8} per year (equivalent to motions of 1 mm/yr on length scales of 100 km); 77% of fatalities in earthquakes occur in areas straining at rates of less than 5×10^{-8} per year (5 mm/yr over 100 km).

FIGURE 4 here, in box

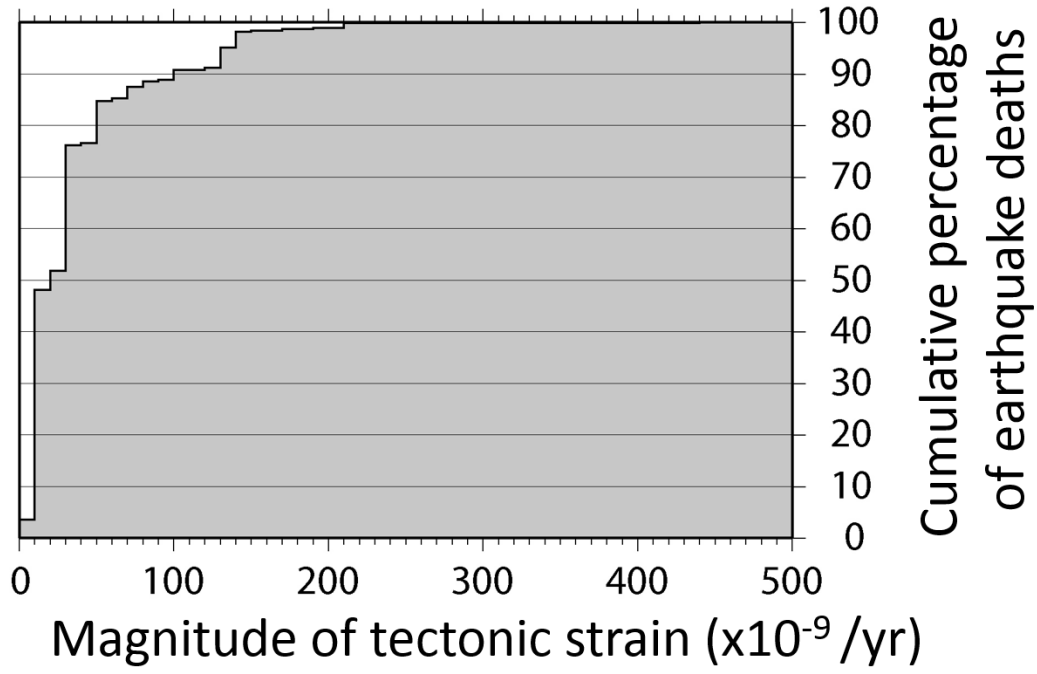

Figure 4: Cumulative histogram comparing the 1.2 million fatalities in onshore earthquakes (USGS, 1900-2010) to geodetic strain rates from the Global Strain Rate Model (Kreemer et al., 2003). 96% of fatalities in earthquakes occur in areas straining at rates higher than 10^{-8} per year; 77% of fatalities occur in areas straining at rates of less than 5 x 10^{-8} per year. Courtesy Matt Garthwaite, Geoscience Australia.

3. Key Observations of Earthquake Cycle Deformation

The last 25 years has seen a dramatic improvement in our ability to measure tectonic deformation using satellite geodesy (Box 1), and the number of observations of time-dependent deformation is now sufficient to describe the general behaviour of typical major fault zones with some degree of confidence (Wright et al., 2013). These patterns of behaviour are ones that any successful model that links surface deformation to seismic hazard must be able to

reproduce or account for. The community typically breaks the quasi-cyclical behaviour of fault zones into three phases: *interseismic*, *coseismic* and *postseismic* deformation. I will do the same, while recognising that interseismic and postseismic deformation may be difficult to separate in many fault zones. I will largely discuss the observations from strike-slip fault zones in the continents, as these have the most comprehensive and highest quality observations at present.

3.1 Interseismic Deformation

Interseismic deformation occurs in the long intervals between earthquakes, once the early transient postseismic deformation (§3.3) has ceased to be clearly observable, and it is thought to reflect the relatively steady motion at depth of the crustal blocks on either side of the fault. In the interseismic time period, faults in the seismogenic upper part of the crust, where earthquakes occur, are locked. However, the blocks continue to move steadily, driven by tectonic forces. This continued motion in the lower crust and mantle causes the upper crust to deform in response. The shape of that deformation tells us about which parts of the crust are moving with the crustal blocks, and at what rate.

One of the most significant findings from satellite geodetic measurements of fault zones is that almost all major strike-slip fault zones show focused strain around them during the interseismic period (Wright et al., 2013). Such deformation can be modelled as if the tectonic block boundaries are simple thin fault zones extending to great depths from the surface, with the entire boundary between blocks displacing at constant rate, except for the locked seismogenic upper crust (Savage and Burford, 1973, Weertman and Weertman, 1966). Reviewing the 131 faults where this model had been used to solve for the thickness of the locked layer, we found that the locking depths were approximately normally distributed with a

mean of 14 km and a standard deviation of 7 km. However, just because this model fits the data doesn't of course mean that it is correct. The elastic earth acts as a natural filter, smoothing out any deformation at depth and limiting our ability to distinguish distributed shear in the lower crust and upper mantle from motion focused entirely on a narrow fault plane; at a typical seismogenic depth of ~15 km, a shear zone below the seismogenic layer that was as wide as 45 km would be indistinguishable from deformation focused on a narrow fault (Moore, 1999). We therefore require independent constraints to determine the width of shear zones beneath the seismogenic upper crust; I will discuss these in sections 4 and 6.

An important question is whether the interseismic deformation that we observe between earthquakes is steady in time, with the rates reflecting the long-term rates of movement between the tectonic blocks separated by the fault. One way of addressing this question is to compare the fault slip rates derived from these simple geodetic models with those derived from geological measurements, in which the fault slip rates are determined by dating surface features that have been offset by movement on the fault. Thatcher (2009) and Meade et al (2013) both carried out such a comparison, and found a good correspondence between the two measurements, given their respective uncertainties; the few outliers that showed significant discrepancies are likely attributable to systematic errors in one or other measurement. This good agreement suggests that any temporal variation is small, and short-term geodetic observations of interseismic deformation can therefore be used to assess the long-term rates of fault motion.

3.2 Coseismic Deformation

Making measurements of the deformation that occurs during earthquakes is now fairly routine, thanks largely to the ability of InSAR to make observations globally without

instruments on the ground (Wright et al., 2013, Weston et al., 2012). The patterns seen in interferograms reveal how the earth deforms during earthquakes in exquisite detail (e.g. Figure 5). The deformation from earthquakes shows that the Earth deforms as an elastic solid on short time scales (seconds – minutes).

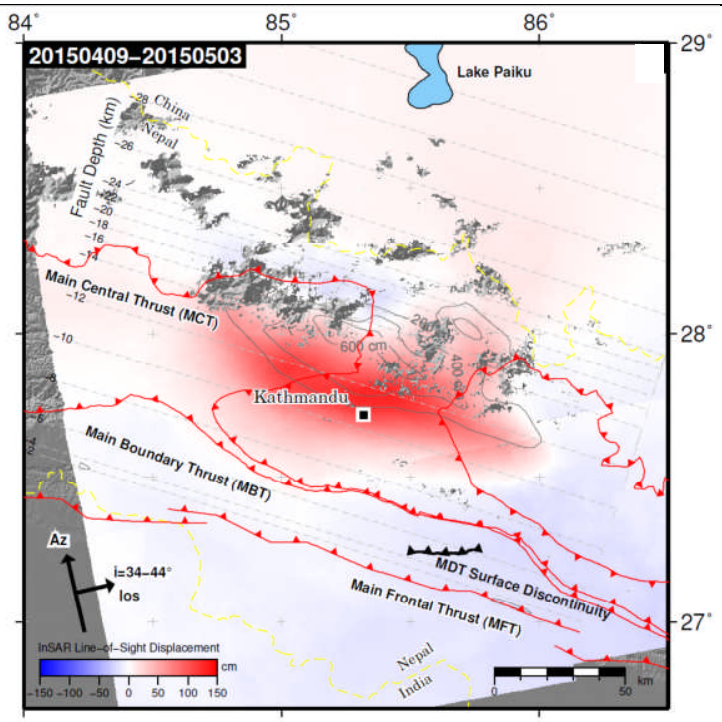

Figure 5: Coseismic displacements for the M7.8 2015 Gorkha (Nepal) earthquake from InSAR measured with the Sentinel-1A satellite using images acquired on 9 April and 3 May 2015. Red colours are motion towards the satellite, whose viewing geometry is shown by the black arrow, and blue colours show motion away from the satellite. The solid contour lines show the magnitude of slip on the fault plane beneath Kathmandu that is required to reproduce the observed surface displacements, with the dashed contour lines showing the depth to the thrust fault. Red lines show mapped surface fault traces – the data clearly show that no significant slip reached the surface in this earthquake. Reproduced from Elliott

(2016).

For moderate to large earthquakes (M6+) in the upper crust, geodetic observations can be used to determine earthquake source geometries and slip distributions (e.g. Figure 6). These source models have some advantages over models derived from traditional seismological methods. Firstly, they provide very accurate location information, particularly if the earthquake is shallow; there are now several examples where InSAR results have led investigators in the field to an earthquake's surface rupture before it was located in the field. Secondly, the source models do not suffer to the same degree from the ambiguity in fault plane inherent in many seismic methods (Biggs et al., 2006). Finally, the distribution of slip on the fault plane can be determined more reliably using geodetic observations than using seismic observations, particularly for shallow earthquakes with magnitudes in the range 6-8 (e.g. Funning et al., 2014). Just a few days after the Nepal earthquake, InSAR observations showed that it had not ruptured the surface. The USGS then updated their estimate of shaking intensity using the geodetic observations; the addition of geodetic data showed that the slip was more concentrated the seismic estimates had suggested. This change in source model caused a significant increase in the USGS estimate of shaking in Kathmandu (Richard Briggs, USGS, pers. comm. 2015).

The primary information we gain on the earthquake deformation cycle from the coseismic phase is on the seismogenic layer thickness. By examining the published geodetic solutions for earthquakes globally, we found that the seismogenic layer thickness is 14 ± 5 km, consistent with the estimate from geodetic observations of interseismic deformation (Wright et al., 2013). We also showed that the depths of earthquakes determined from geodesy were consistent with

those determined from seismology, which confirms that the much larger catalogue of earthquake depths determined from seismic source modelling is reliable. Source models from seismology show that there are some regional variations in seismogenic layer thickness. Most seismogenic areas of the continents have seismogenic thicknesses consistent with the global average of ~15 km, meaning only the upper crust if involved in earthquakes. But in some areas, such as the Tien Shan and parts of the East African Rift, the seismogenic layer thickness is similar to the thickness of the crust, which can result in much larger earthquakes that rupture the entire crust (e.g. Jackson et al., 2008).

3.3 Postseismic Deformation

Following earthquakes, a transient phase of postseismic deformation often occurs (Wright et al., 2013). This is thought to arise as the crust and mantle adjust to the coseismic stress changes; the distribution of this deformation in space and time provides key data with which to test models of the earthquake cycle. Postseismic deformation has been observed following about 25 continental earthquakes. In some cases, the deformation is comparable in magnitude to the deformation that occurs during earthquakes, but in other cases it is a small fraction of the coseismic deformation (Fattahi et al., 2015). In Wright et al. (2013) we reviewed geodetic studies of postseismic deformation. In about 60% of earthquakes where postseismic deformation had been observed, deformation was found very close to the fault rupture, implying shallow processes. In 75% of earthquakes, deformation was observed over a broad region surrounding the fault plane, implying motion beneath the seismogenic layer. Rates of postseismic deformation have been observed to decay over time periods of months to years, with most observations spanning the first few years following major earthquakes. In a few cases, long-lived postseismic deformation has been invoked to explain deformation

signals around faults that are still observed several decades after major earthquakes (e.g. Gourmelen and Amelung, 2005).

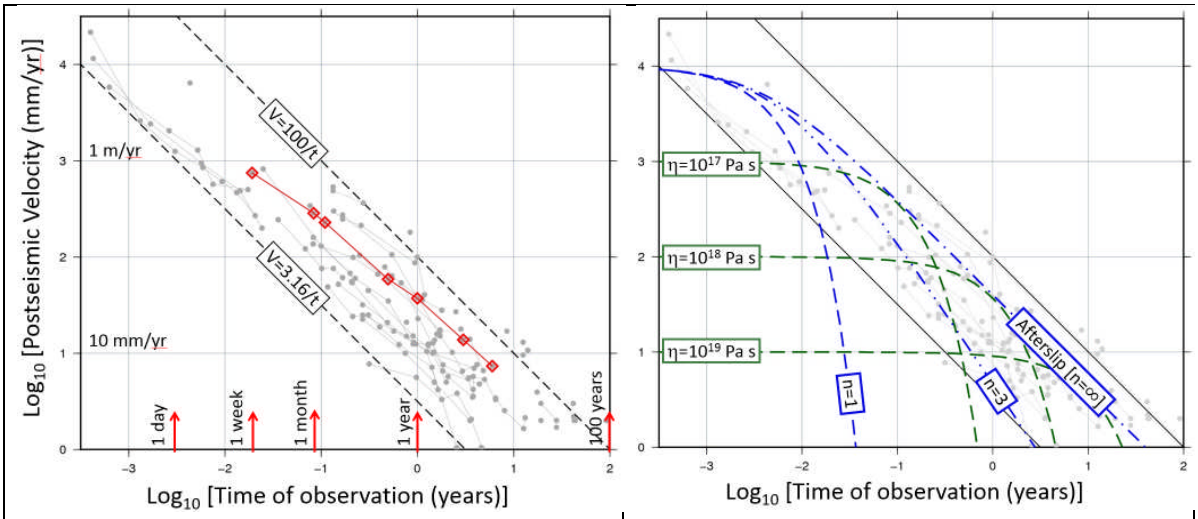

Figure 6: [*Left*] Compilation of postseismic velocities measured with geodesy for all earthquakes in the literature as a function of time since the earthquake. Maximum velocities observed are shown at the time of observation. Where points are linked, these are for the same earthquake. Postseismic velocities following the Izmit earthquake are highlighted in red. [*Right*] Simple models for postseismic velocity. Green dashed curves show velocities predicted for a linear Maxwell viscoelastic model with viscosities of η=10^{17}, 10^{18} and 10^{19} Pa s, and an initial displacement of 1 m. Blue curves show predicted displacements for a non-linear visco-elastic shear zone, with stress exponents of n=1, 3 and ∞, using the formulation of Marone (1998), with an initial velocity of 10^4 mm/yr and a relaxation time of 0.004 years. The power-law solution for n=∞ is identical to the solution for steady-state afterslip predicted by rate and state friction; the solution for n=1 is equivalent to the linear Maxwell case with viscosity of 4 x 10^{15} Pa s. Adapted from Ingleby and Wright (in prep for GRL 2016).

A variety of models have been used to try to explain observations of postseismic deformation (Box 2). However, because different authors have tackled this problem with different prejudices and assumptions, it has been difficult to assess what the data are actually telling us. To address this, my student Tom Ingleby has returned to the direct observations of postseismic deformation. He has extracted estimates of the maximum postseismic velocity from the published literature, and examined how these vary as a function of time since the earthquake (Ingleby and Wright, In Prep for *Geophysical Research Letters*). These show a remarkably simple pattern (Figure 6), with postseismic velocities decreasing with increasing time; there is a linear relationship on a log-log plot with a slope of -1, indicating that velocity is inversely proportional to the time since the earthquake. This relationship holds for individual earthquakes of all mechanisms, with a factor of 30-40 separating the earthquakes with the fastest rates of deformation from those with the slowest. This compilation suggests that the transient deformation following earthquakes is measurable (> 1 mm/yr) for between ~3 and 100 years after an earthquake. Amongst the mechanisms that have been proposed for postseismic deformation (Box 2), a ~1/t dependence of postseismic velocity is predicted by afterslip models using rate and state friction laws, and by viscoelastic relaxation models in which stress and strain in the viscous material are related through a power-law relationship between stress and strain rate, with stress exponent, n, greater than 3 (Marone, 1998; Figure 6). Viscoelastic models with a single linear (Newtonian) viscosity beneath an elastic lid cannot explain the entire time series – relatively low viscosities are required to explain the initial period of postseismic deformation, with higher viscosities needed to fit the velocities observed later after the earthquake. Viscoelastic models with Burgers-type materials, which have two

effective relaxation times, can fit the overall scatter of observations, but do not reproduce the ~1/t relationship seen for individual earthquakes.

Box 2: Mechanisms of postseismic deformation

Three primary mechanisms are thought to be responsible for postseismic deformation. Firstly, parts of the fault plane can continue to slip aseismically following earthquakes. This *afterslip* is controlled by friction. Earthquakes occur on parts of the fault plane where the dynamic coefficient of friction is lower than the static one, with slip accelerating once it has started; afterslip is thought to occur where the dynamic co-efficient of friction is higher than the static one, meaning stable slip can occur (e.g. Scholz, 2002). Geodetic inversions of the spatial distribution of afterslip usually show that it occurs on areas of the fault that are distinct from those that failed in the earthquake, with afterslip often found to occur above or below the fault's main slip patch.

The second way in which the Earth adjusts during the postseismic period is through viscous flow of the lower crust and upper mantle. This flow is controlled by grain-scale mechanisms within crystals, such as dislocation and diffusion creep. The rates at which these mechanisms allow the solid Earth to deform, and which mechanisms dominate in given conditions, depend on stress, temperature, pressure, water content, and grain size, as well as the chemical composition of the material (Burgmann and Dresen, 2008). In general, flow becomes easier (effective viscosity becomes lower) as the crust/mantle becomes hotter and wetter. Dislocation creep, for which strain rate has a non-linear dependence on stress, occurs at high stresses and/or if the crystal grain sizes are large; diffusion creep, where strain rate and stress are linearly related, occurs at relatively low stresses and/or if crystal grain sizes are small.

A final mechanism that has been invoked to explain some observations of postseismic deformation is *poroelastic* deformation, which results from the flow of pore-fluids in response to coseismic deformation. Poroelastic deformation was most clearly observed after two moderate earthquakes in Iceland in June 2000 (Jonsson et al., 2003), where independent observations from hydrothermal water wells could confirm that water was flowing. During the earthquakes, the water level rose in wells that were in regions around the fault that contracted, and dropped in wells that were in regions that dilated. In the three months that followed the earthquake, water in the areas that contracted during the earthquake flowed to the areas that dilated, reversing the initial change seen in the wells. This flow of water caused surface deformation to occur in sync with the flow, with a spatial pattern identical to that predicted from models of poroelastic deformation. This mechanisms has been invoked in a few other earthquakes, but is likely to be responsible only for short-lived postseismic deformation.

3.4 Co-located observations of all three phases of deformation

So far, I have discussed observations of individual phases of the earthquake cycle separately; to build a model from such observations requires us to assume that faults in all parts of the world behave in a similar manner. There are, however, a few faults where we don't need to make these assumptions – faults where interseismic deformation was measured late in the earthquake cycle, the coseismic deformation was measured during a major earthquake, and postseismic deformation has been observed in the years following the earthquake. For continental strike-slip faults, which are the primary focus here, we have observations of these three phases for the Denali Fault in Alaska, the Parkfield section of the San Andreas Fault, the Manyi Fault in Tibet, and the Izmit section of the North Anatolian Fault in Turkey. All of these

faults showed focused interseismic strain preceding a major earthquake, and a period of rapid postseismic deformation following the earthquake.

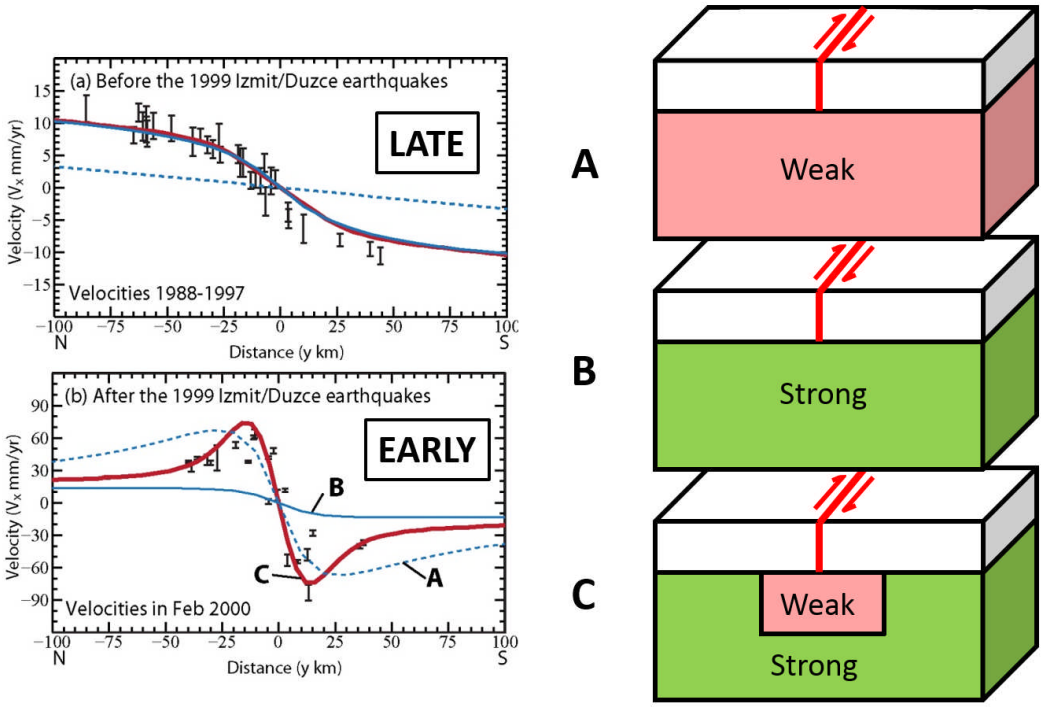

Figure 7: Profile of fault-parallel velocities (black error bars) along the centre of the 1999 Izmit earthquake rupture, measured with GNSS before (top) and 6 months after (bottom) the earthquake. The three model curves correspond to the cartoon configurations of crustal viscosities shown in the right-hand panel. Figure adapted from Yamasaki, Wright and Houseman (2014).

The best of these data sets is from the Izmit section of North Anatolian Fault (Figure 7), which failed in two M7+ earthquakes in 1999 (Yamasaki et al., 2014). In the decade before the earthquake, McClusky et al. (2000) collected GPS observations that constrain the interseismic

deformation. Numerous authors used InSAR and GPS to measure the coseismic deformation during the 1999 earthquakes (e.g. Feigl et al., 2002); Ergintav et al. (2009) have continued to track postseismic deformation using GPS. Before 1999, strain was focused in a ~50-km-wide region around the fault, consistent with the elastic dislocation models discussed in §3.1. After the earthquake, a period of rapid postseismic adjustment took place, with postseismic velocities 6 months after the earthquake of ±60 mm/yr measured at distances 10-15 km from the fault. These velocities have decayed with the characteristic ~1/t dependency since the earthquake (Figure 5).

4. Models of earthquake cycle deformation

The simplest model of the full earthquake deformation cycle for strike-slip faults consists of regularly repeating earthquakes that rupture an infinitely-long fault in an elastic lid overlying a viscoelastic substrate (Savage, 2000, Savage and Prescott, 1978). In this *viscoelastic coupling* model, the upper blocks slide past each other in the long term, but are locked together at the fault between events. The deformation that we see at the surface depends on distance to the fault, the time since the most recent earthquake, and the ratio, τ, of the relaxation time of the viscoelastic substrate to the time interval between the repeating earthquakes. If τ is small, the substrate is weak, relaxing any postseismic stresses completely between earthquakes (model A in Figure 7). For values of τ that approach or exceed 1, the substrate is relatively strong; postseismic stresses will not completely relax between events (model B in Figure 7).

Viscoelastic coupling models with a weak substrate can reproduce observations of rapid postseismic transient deformation. However, they do not predict focused interseismic deformation late in the earthquake cycle; there is no reason for strain to be focused around the

fault. By contrast, models with a strong substrate cannot produce rapid postseismic transients – the substrate is simply too stiff to relax quickly. However, because postseismic stresses do not fully relax between earthquakes, models with strong substrates are able to produce focused interseismic strain late in the cycle, with the same arctangent shape as a purely elastic deformation model (Figure 7).

In the simple two-layer viscoelastic coupling model, there is no single value of τ that is capable of reproducing both rapid postseismic transients and focused interseismic strain – we need multiple relaxation times. One popular way of solving this problem is to use a material law that explicitly allows for multiple relaxation times, such as a standard linear solid or Burgers flow law (Hetland and Hager, 2005). These two-layer models can reproduce observations of rapid postseismic deformation transients and focused interseismic deformation, if tuned correctly. However, they do not reproduce the observed ~1/t decay in postseismic velocities, and the distribution of material properties is somewhat arbitrary.

One clear limitation of the viscoelastic coupling model, and the other models discussed above, is that they ignore spatial variations in material properties around fault zones. There are numerous reasons why the strength of rocks in the deep roots of faults is likely to be different to that of the surrounding crust: there are likely to be different lithologies with different properties within fault zones; heat created by shearing will lower the viscosity; higher stresses will also cause weakening if the materials are in the nonlinear deformation regime; grain sizes may be reduced because of shearing, also causing weakening; and there may be increased water content due to fluid flow through the fault zones. Most of these processes are likely to result in a weak zone in the deep roots of faults. Recently, we tried to incorporate this geological complexity into a model of the full earthquake cycle, while trying to maintain the

relative simplicity of the viscoelastic coupling model (Yamasaki et al., 2014). In our *weak zone* model (model C in Figure 7), we embedded a weaker region (low τ) within a stronger substrate (high τ). Following an earthquake, relaxation of the weak zone reproduces the observed rapid postseismic transients. The stronger substrate does not relax fully between earthquakes, allowing the model to reproduce focused interseismic strain late in the cycle. For the North Anatolian Fault, this model provides a minimum value for the viscosity of the background substrate of ~10^{20} Pa s. The estimate of viscosity in the weak zone is ~2 orders of magnitude lower, at ~10^{18} Pa s. We were also able to place some loose bounds on the dimensions of the weak zone, finding it to be between 10 and 20 km thick, and between 10 and 40 km wide. However, because deformation at the surface is caused by the relaxation of two linear materials, this model also cannot reproduce the ~1/t decay observed for postseismic velocities; further modification of the flow law within the weak zone, for example the introduction of a power-law relationship between stress and strain, could solve this problem.

An alternative approach has been to try to predict the behaviour of fault zones using our best geological knowledge of the composition of crust and mantle, our best understanding from geophysical studies of the rate that temperature increases with depth, and our best understanding from rock mechanics experiments of how earth materials deform under the stresses and temperature conditions they experience within the Earth. This approach is challenging because the knowledge needed to make such a prediction is imperfect, and the resulting models are complex, involving variations in material properties and physical conditions in space and time. The most comprehensive attempt to produce such a model is from Takeuchi and Fialko (2012). For realistic geological materials, they find that strain localises in the viscoelastic substrate due to shear heating and the power-law dependence of

strain rate on stress, effectively producing a weak zone under the fault that is able to relax quickly during the postseismic period. Takeuchi and Fialko suggest that long-term strain is localised in a shear zone in the lower crust that is 3-5 km wide. Although they don't plot the time-dependence of postseismic velocity predicted by their model, a power-law shear zone would reproduce the observed ~1/t time dependence (Figure 6; Marone, 1998) if the stress exponent is greater than ~3.

Unfortunately, we cannot consider this problem solved. An entirely different class of models is also capable of explaining the observations of earthquake cycle deformation without any viscoelastic relaxation, using only fault friction. In such models, only a small part of the fault fails during earthquakes – the fault plane continues at depth below the seismogenic part of the crust. The portion of the fault that fails in earthquakes has unstable, velocity-weakening coefficients of friction (Box 2); the remainder of the fault has velocity-strengthening friction, and can slide steadily during the interseismic and postseismic intervals. Tse and Rice (1986) built the first complete earthquake cycle model based on this type of friction, using a specific lab-based friction law known as rate and state friction. Their model, in which fault properties only vary with depth, predicts an accelerated period of shallow and deep afterslip in the velocity-strengthening regions following periodic earthquakes in the upper layer. Barbot et al. (2012) developed a more sophisticated version of the same model in which frictional properties vary in two dimensions on the fault plane. They applied this model to the Parkfield section of the San Andreas Fault, which has a relatively short inter-event time, and were able to reproduce seismic and geodetic observations of the full earthquake cycle. Models of the earthquake cycle that use rate and state friction also predict the ~1/t dependence of postseismic velocities (Figure 6; Marone, 1998).

Both viscoelastic and frictional models of the earthquake deformation cycle can explain geodetic observations of focused interseismic deformation late in the cycle and rapid postseismic transients. Although significant parts of the literature are devoted to testing which of these models is most appropriate, both mechanisms are almost certainly operating in some form. We know that frictional afterslip certainly occurs on the shallow portions of some faults (e.g. Elliott, 2015), and it seems likely that velocity-strengthening conditions also exist on the deepest parts of faults (Tse and Rice, 1986). Observations of glacial isostatic adjustment (e.g. King et al., 2010) are hard to explain without having viscoelastic relaxation occurring at some depths within the earth, and lab experiments of rock properties also predict that viscoelastic relaxation mechanisms should be important for the deformation we see in the earthquake deformation cycle (Burgmann and Dresen, 2008).

My motivation for attempting to understand the earthquake deformation cycle is to allow us to use short-term geodetic observations to constrain seismic hazard. If both viscoelastic and frictional deformation mechanisms are operating, it makes it extremely challenging to build a model that is useful for this purpose – there are too many unknowns with too few observational constraints. However, there is some hope. Despite the radically different mechanisms that operate, there are commonalities between the models that fit the geodetic observations. Firstly, viscoelastic and frictional approaches both require a “strong” substrate away from the fault zone in order to explain focused interseismic deformation late in the cycle. In the case of the elastic model, the material is an elastic solid that cannot undergo permanent deformation. For viscoelastic models, the material away from fault zones can deform but it has a relaxation time that is comparable to, or larger than, the inter-event time; it is slow relaxation of this material that leads to the surface observations of focused strain late in the cycle. Secondly, both

approaches predict narrow zones of finite strain in the lower crust. For frictional models, the fault simply continues beneath the seismogenic layer. For viscoelastic models, strain is focused beneath the fault as a result of depth-dependent viscosity, shear heating, and the power-law rheology, such that the finite strain is predicted to occur within a zone that may only be a few kilometres wide (Moore and Parsons, 2015); postseismic deformation would still occur in a broader weak zone, if viscosities are lowered due to shear heating. Finally, the requirement for postseismic velocities to be inversely proportional to the time since the last earthquake is met by models of frictional afterslip that use rate and state friction laws, and by models of viscoelastic relaxation that use a power-law relationship between stress and strain rate (Marone, 1998). This latter agreement is critical for the use of geodesy for seismic hazard - it means that any measureable postseismic transient deformation will have decayed within ~3 to 100 years of the most recent earthquake (Figure 6). This is a small fraction of the inter-event time for most faults in the continents and for any faults that have experienced recent earthquakes we can use the temporal behaviour to make informed empirical or model-based corrections to strain data to account for postseismic deformation. Short-term measurements of geodetic strain are therefore telling us about the long-term accumulation of strain energy, and can be used to improve estimates of seismic hazard.

5. Towards a practical seismicity forecast from geodetic strain

I have hopefully convinced you of the utility of short-term geodetic measurements of strain in terms of informing models of seismic hazard. Bird and Kreemer (2015) set out to assess, in practice, how well seismic hazard models derived from the best-available geodetic strain data

compare with predictions based purely on a seismic catalogue. To convert geodetic strain rate into seismicity rate we need to make four major assumptions. Firstly, we need to prescribe the style of faulting that is likely to occur in each region – the same strain can be accommodated by different combinations of faults. Bird and Kreemer do this by using a set of rules to ascribe the most comparable class of plate boundary for each deforming region, as laid out in Bird and Liu (2007). Secondly, we need to know how thick the seismogenic layer is. This can be achieved by looking at the depths of earthquakes in any region. Thirdly, we need to know the relative numbers of earthquake of different sizes – a few large earthquakes can cause the same amount of deformation as many large ones. The Gutenberg-Richter law relates the relative number of large earthquakes to small ones; this law states that for each decrease in earthquake magnitude (e.g. from M7 to M6) there are ~10 times more earthquakes (Scholz, 2002). Finally, we need to know the proportion of strain that is accommodated without earthquakes, for example through fault creep or distributed plastic deformation. Bird and Kreemer calibrate their forecast for different tectonic regimes using seismicity data; this also soaks up any errors in other assumptions, such as the dips of faults or layer thickness. After implementing these assumptions and calibrations, they used the strain rate model to forecast seismicity rates between 2005 and 2012, a period they had excluded from their calibration (Figure 8). For continental regions, the tuning factor was ~1 – i.e. all geodetic strain is released as earthquakes. They found that their strain-rate-derived forecast was as successful as comparable model derived independently from seismicity data.

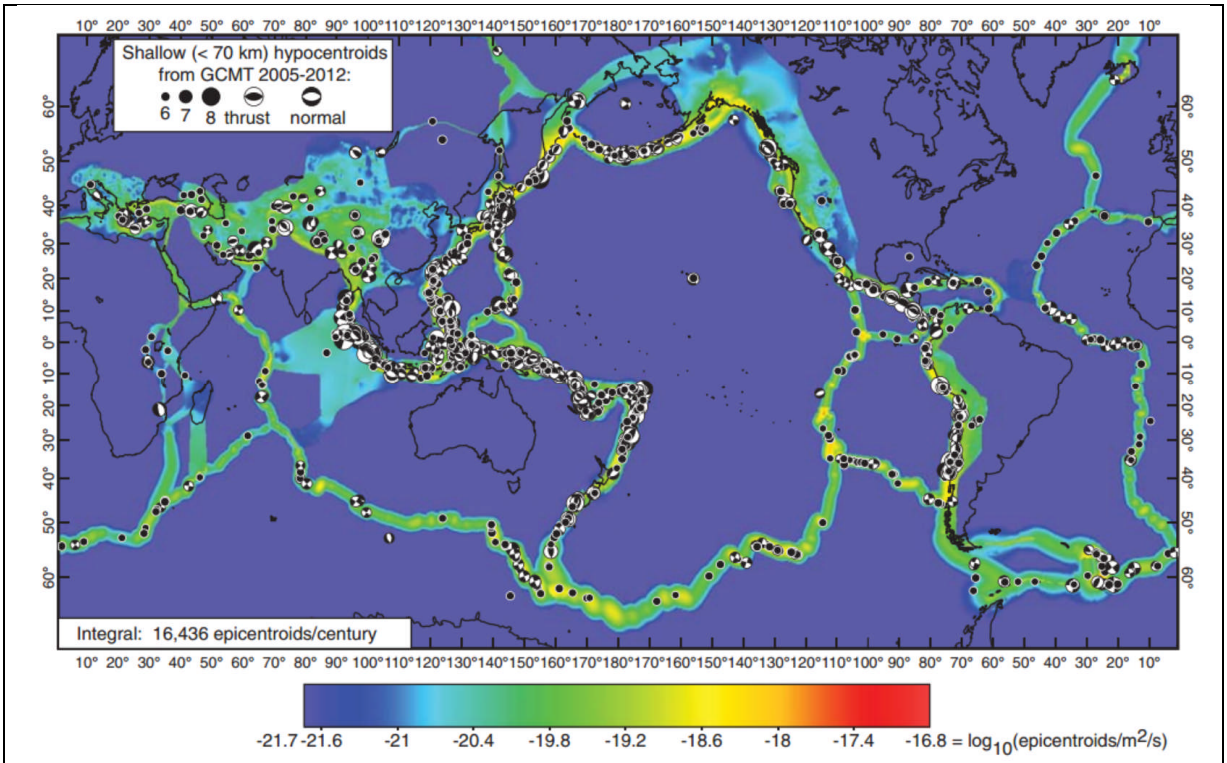

Figure 8: *[Could be cut if you think we have too many figures already]* Bird and Kreemer (2015) seismicity rate forecast based on a global strain model derived from GNSS data, compared to M6+ earthquakes that occurred between 2005 and 2012 in the Global CMT catalogue. The forecast is for earthquakes with M > 5.767; for reference, an earthquake rate of $\log_{10}$(epicentroids/m^2/s) = -19.5 (green on the figure) corresponds to one earthquake per century in a 100 x 100 km box. Figure from Bird and Kreemer (2015).

Future improvements in the quality and spatial resolution of geodetic strain data (Box 1) will lead to improvements in the geodesy-based seismic hazard forecasts. I would advocate an approach that integrates geodetic data with instrumental and historical records of seismicity (e.g. Bird et al., 2015), along with longer-term histories of fault activity that are derived from palaeoseismology and tectonic geomorphology. The Global Earthquake Model, a partnership

funded jointly by the public sector and the insurance industry, is taking exactly this approach in the derivation of its future seismic hazard models.

6. Implications for the deep structure of faults and the strength of continental lithosphere.

The improved understanding of the earthquake deformation cycle that I set out here has implications beyond seismic hazard for the deep structure of faults and the strength of continental lithosphere.

The degree to which strain is focused in the lower crust and mantle beneath active faults has been the subject of much debate. For major strike-slip faults, the story from geodetic observations and models of earthquake cycle deformation is now fairly clear. The observations of focused interseismic strain late in the cycle and the ~1/t dependence of postseismic deformation transients both require strain to be focused into relatively narrow shear zones below the seismogenic crust. This conclusion agrees with geological observations of exhumed shear zones, where several examples document structures associated with relatively narrow zones of finite strain. Testing this hypothesis using seismic imaging techniques has been more challenging. Existing images of the lower crust beneath the surface expression of the San Andreas Fault, for example, are relatively low resolution, but also suggest a relatively narrow shear zone at depth beneath the main branch of the San Andreas Fault. With colleagues in Leeds, Aberdeen and at the Kandilli Observatory in Istanbul, we have been conducting a high-resolution seismic experiment to image the deep structure of the North Anatolian Fault in the location that failed in the 1999 earthquakes (DANA, 2012). Preliminary results from receiver

functions also suggest sharp changes in crustal properties across the two major fault strands in the location of the survey (Kahraman et al., 2015). Further work is needed to understand how such shear zones develop, and whether similar weak zones exist under extensional and thrust faults in the continents.

Another major debate in the last decade has concerned the strength of the continental lithosphere. In one view, the strength of the continents lies primarily in the upper seismogenic layer (Jackson et al., 2008), the so-called *crème brulée* model. Alternatively, it has been argued that considerable strength also lies in the mantle, with a weak lower crust in between these two strong layers; this is often referred to as a *jelly sandwich* model (Burov and Watts, 2006). The low viscosities obtained from postseismic studies and the relationship between seismogenic layer thickness and some estimates of elastic thickness support the *crème brulée* model. I have shown here that major faults modify the crust beneath the seismogenic layer, creating weak zones that have much weaker material properties. Therefore, any strength estimates derived from studies around major faults are only telling us about the strength of the fault zone, not of the surrounding lithosphere. Earthquake cycle deformation requires a relatively strong lower crust, except near major faults – Burgmann and Dresen (2008) describe such a configuration as *banana split* model. Watts et al. (2013) compare the response of the lithosphere to loading on different timescales, suggesting that the effective thickness of the load-bearing elastic outer layer reduced as the length of observation increased. Postseismic deformation is an anomaly in this general pattern, with very thin elastic layers found for very short time periods of observation. This makes more sense if postseismic observations are only telling us about fault zones, and not about the general strength of the lithosphere.

7. Conclusions and future perspectives

I have shown that geodetic data provides a useful complementary approach for understanding seismic hazard. By examining observations of time-dependent deformation associated with the earthquake deformation cycle, we can be confident that short-term geodetic observations are telling us about the long-term accumulation of strain energy around faults, and are only biased if we are in the immediate postseismic period following major earthquakes. Although scientists have known about the link between strain and earthquakes for more than 100 years, this approach is now finally coming of age.

Over the next decade, we will see further dramatic improvement in our ability to measure tectonic deformation using satellite geodetic techniques, particularly from the combination of InSAR and GPS (Box 1). In COMET (http://comet.nerc.ac.uk), we are building a system to systematically process InSAR data acquired by the EU's Sentinel-1 satellites. The aim is to produce high-resolution, accurate deformation data for all the tectonic and volcanic areas of the planet, and to use these to help constrain future hazard models.

Acknowledgements.

This review summarises work conducted collaboratively with colleagues in the UK Natural Environment Research Council's Centre for the Observation and Modelling of Earthquakes, Volcanoes and Tectonics (COMET). I have tried to credit individual collaborators as appropriate, and take all the blame for the wilder interpretations. I'd like to thank Tony Watts for my nomination for the Bullerwell lectureship, and members of the BGA board for supporting it.

References

AMBRASEYS, N. & BILHAM, R. 2011. Corruption kills. *Nature,* 469**,** 153-155.

BARBOT, S., LAPUSTA, N. & AVOUAC, J.-P. 2012. Under the hood of the earthquake machine: toward predictive modeling of the seismic cycle. *Science,* 336**,** 707-710.

BIGGS, J., BERGMAN, E., EMMERSON, B., FUNNING, G., JACKSON, J., PARSONS, B. & WRIGHT, T. 2006. Fault identification for buried strike-slip earthquakes using InSAR: The 1994 and 2004 Al Hoceima, Morocco earthquakes. *Geophysical Journal International,* 166**,** 1347-1362.

BIRD, P., JACKSON, D., KAGAN, Y., KREEMER, C. & STEIN, R. 2015. GEAR1: A global earthquake activity rate model constructed from geodetic strain rates and smoothed seismicity. *Bulletin of the Seismological Society of America,* 105**,** 2538-2554.

BIRD, P. & KREEMER, C. 2015. Revised tectonic forecast of global shallow seismicity based on version 2.1 of the Global Strain Rate Map. *Bulletin of the Seismological Society of America,* 105**,** 152-166.

BIRD, P. & LIU, Z. 2007. Seismic hazard inferred from tectonics: California. *Seismological Research Letters,* 78**,** 37-48.

BLEWITT, G. 2007. GPS and space-based geodetic methods. *Treatise on Geophysics,* 3**,** 351-390.

BURGMANN, R. & DRESEN, G. 2008. Rheology of the lower crust and upper mantle: Evidence from rock mechanics, geodesy, and field observations. *Annual Review of Earth and Planetary Sciences,* 36**,** 531-567.

BURGMANN, R., ROSEN, P. & FIELDING, E. 2000. Synthetic aperture radar interferometry to measure Earth's surface topography and its deformation. *Annual Review of Earth and Planetary Sciences,* 28**,** 169-209.

BUROV, E. & WATTS, A. 2006. The long-term strength of continental lithosphere:" jelly sandwich" or" crème brûlée"? *GSA today,* 16**,** 4.

DANA 2012. Dense Array for North Anatolia. International Federation of Digital Seismograph Networks.

ELLIOTT, J. 2016. Nepal Earthquake Paper. *Nature Geoscience,* In Press.

ELLIOTT, J. R., A. J. ELLIOTT, A. HOOPER, Y. LARSEN, P. MARINKOVIC, AND T. J. WRIGHT 2015. Earthquake monitoring gets boost from new satellite. *Eos,* 96.

ERGINTAV, S., MCCLUSKY, S., HEARN, E., REILINGER, R., CAKMAK, R., HERRING, T., OZENER, H., LENK, O. & TARI, E. 2009. Seven years of postseismic deformation following the 1999, M=7.4 and M=7.2, Izmit-Duzce, Turkey earthquake sequence. *Journal of Geophysical Research-Solid Earth,* 114.

FATTAHI, H., AMELUNG, F., CHAUSSARD, E. & WDOWINSKI, S. 2015. Coseismic and postseismic deformation due to the 2007 M5. 5 Ghazaband fault earthquake, Balochistan, Pakistan. *Geophysical Research Letters*.

FEIGL, K. L., SARTI, F., VADON, H., MCCLUSKY, S., ERGINTAV, S., DURAND, P., BÜRGMANN, R., RIGO, A., MASSONNET, D. & REILINGER, R. 2002. Estimating slip distribution for the Izmit mainshock from coseismic GPS, ERS-1, RADARSAT, and SPOT measurements. *Bulletin of the Seismological Society of America,* 92**,** 138-160.

FUNNING, G. J., FUKAHATA, Y., YAGI, Y. & PARSONS, B. 2014. A method for the joint inversion of geodetic and seismic waveform data using ABIC: application to the 1997 Manyi, Tibet, earthquake. *Geophysical Journal International***,** ggt406.

GOLDSTEIN, R. M. & ZEBKER, H. 1987. Interferometric radar measurement of ocean surface currents.

GOURMELEN, N. & AMELUNG, F. 2005. Postseismic mantle relaxation in the central Nevada seismic belt. *Science,* 310**,** 1473-1476.

HETLAND, E. A. & HAGER, B. H. 2005. Postseismic and interseismic displacements near a strike-slip fault: A two-dimensional theory for general linear viscoelastic rheologies. *J. Geophys. Res.,* 110**,** B10401.

JACKSON, J. 2001. Living with earthquakes: know your faults. *Journal of Earthquake Engineering,* 5**,** 5-123.

JACKSON, J., MCKENZIE, D., PRIESTLEY, K. & EMMERSON, B. 2008. New views on the structure and rheology of the lithosphere. *Journal of the Geological Society,* 165**,** 453-465.

JONSSON, S., SEGALL, P., PEDERSEN, R. & BJÖRNSSON, G. 2003. Post-earthquake ground movements correlated to pore-pressure transients. *Nature,* 424**,** 179-183.

KAHRAMAN, M., CORNWELL, D. G., THOMPSON, D. A., ROST, S., HOUSEMAN, G. A., TÜRKELLI, N., TEOMAN, U., POYRAZ, S. A., UTKUCU, M. & GÜLEN, L. 2015. Crustal-scale shear zones and heterogeneous structure beneath the North Anatolian Fault Zone, Turkey, revealed by a high-density seismometer array. *Earth and Planetary Science Letters,* 430**,** 129-139.

KING, M. A., ALTAMIMI, Z., BOEHM, J., BOS, M., DACH, R., ELOSEGUI, P., FUND, F., HERNÁNDEZ-PAJARES, M., LAVALLEE, D. & CERVEIRA, P. J. M. 2010. Improved constraints on models of glacial isostatic adjustment: a review of the contribution of ground-based geodetic observations. *Surveys in geophysics,* 31**,** 465-507.

KREEMER, C., BLEWITT, G. & KLEIN, E. C. 2014. A geodetic plate motion and global strain rate model. *Geochemistry, Geophysics, Geosystems,* 15**,** 3849-3889.

KREEMER, C., HOLT, W. E. & HAINES, A. J. 2003. An integrated global model of present-day plate motions and plate boundary deformation. *Geophysical Journal International,* 154**,** 8-34.

MARONE, C. 1998. Laboratory-derived friction laws and their application to seismic faulting. *Annual Review of Earth and Planetary Sciences,* 26**,** 643-696.

MASSONNET, D. & FEIGL, K. L. 1998. Radar interferometry and its application to changes in the Earth's surface. *Reviews of Geophysics,* 36**,** 441-500.

MASSONNET, D., ROSSI, M., CARMONA, C., ADRAGNA, F., PELTZER, G., FEIGL, K. & RABAUTE, T. 1993. The displacement field of the Landers earthquake mapped by radar interferometry. *Nature,* 364**,** 138-142.

MCCLUSKY, S., BALASSANIAN, S., BARKA, A., DEMIR, C., ERGINTAV, S., GEORGIEV, I., GURKAN, O., HAMBURGER, M., HURST, K., KAHLE, H., KASTENS, K., KEKELIDZE, G., KING, R., KOTZEV, V., LENK, O., MAHMOUD, S., MISHIN, A., NADARIYA, M., OUZOUNIS, A., PARADISSIS, D., PETER, Y., PRILEPIN, M., REILINGER, R., SANLI, I., SEEGER, H., TEALEB, A., TOKSOZ, M. N. & VEIS, G. 2000. Global Positioning System constraints on plate kinematics and dynamics in the eastern Mediterranean and Caucasus. *Journal of Geophysical Research-Solid Earth,* 105**,** 5695-5719.

MISRA, P. & ENGE, P. 2006. *Global Positioning System: Signals, Measurements and Performance Second Edition*, Lincoln, MA: Ganga-Jamuna Press.

MOORE, J. D. & PARSONS, B. 2015. Scaling of viscous shear zones with depth-dependent viscosity and power-law stress–strain-rate dependence. *Geophysical Journal International,* 202**,** 242-260.

MOORE, M. A. 1999. *Crustal deformation in the southern New Zealand region.* D.Phil., University of Oxford.

PELTZER, G., CRAMPÉ, F., HENSLEY, S. & ROSEN, P. 2001. Transient strain accumulation and fault interaction in the Eastern California shear zone. *Geology,* 29**,** 975-978.

REID, H. F. 1910. *The mechanics of the earthquake: the California earthquake of 18 April, 1906. Report of the State Earthquake Investigation Commission, no. 2.*, Carnegie institution of Washington.

REITER, L. 1991. *Earthquake hazard analysis: issues and insights*, Columbia University Press.

SAVAGE, J. 2000. Viscoelastic-coupling model for the earthquake cycle driven from below. *Journal of Geophysical Research-Solid Earth,* 105**,** 25525-25532.

SAVAGE, J. & BURFORD, R. O. 1973. Geodetic Determination of Relative Plate Motion in Central California. *Journal of Geophysical Research,* 78**,** 832-845.

SAVAGE, J. & PRESCOTT, W. 1978. Asthenosphere readjustment and the earthquake cycle. *Journal of Geophysical Research,* 83**,** 3369-3376.

SCHOLZ, C. H. 2002. *The mechanics of earthquakes and faulting*, Cambridge university press.

SIEBERT, L. & SIMKIN, T. 2014. Volcanoes of the world: an illustrated catalog of Holocene volcanoes and their eruptions.

STEIN, S., GELLER, R. J. & LIU, M. 2012. Why earthquake hazard maps often fail and what to do about it. *Tectonophysics,* 562**,** 1-25.

TAKEUCHI, C. S. & FIALKO, Y. 2012. Dynamic models of interseismic deformation and stress transfer from plate motion to continental transform faults. *Journal of Geophysical Research,* 117**,** B05403.

TSE, S. T. & RICE, J. R. 1986. Crustal earthquake instability in relation to the depth variation of frictional slip properties. *Journal of Geophysical Research: Solid Earth (1978–2012),* 91**,** 9452-9472.

WALKER, R., WEGMANN, K., BAYASGALAN, A., CARSON, R., ELLIOTT, J., FOX, M., NISSEN, E., SLOAN, R., WILLIAMS, J. & WRIGHT, E. 2015. The Egiin Davaa prehistoric rupture, central Mongolia: a large magnitude normal faulting earthquake on a reactivated fault with little cumulative slip located in a slowly deforming intraplate setting. *Geological Society, London, Special Publications,* 432**,** SP432. 4.

WATTS, A., ZHONG, S. & HUNTER, J. 2013. The behavior of the lithosphere on seismic to geologic timescales. *Annual Review of Earth and Planetary Sciences,* 41**,** 443-468.

WEERTMAN, J. & WEERTMAN, J. R. 1966. Elementary dislocation theory.

WESTON, J., FERREIRA, A. M. & FUNNING, G. J. 2012. Systematic comparisons of earthquake source models determined using InSAR and seismic data. *Tectonophysics*.

WITHAM, C. 2005. Volcanic disasters and incidents: a new database. *Journal of Volcanology and Geothermal Research,* 148**,** 191-233.

WRIGHT, T., PARSONS, B. & FIELDING, E. 2001. Measurement of interseismic strain accumulation across the North Anatolian Fault by satellite radar interferometry. *Geophysical Research Letters,* 28**,** 2117-2120.

WRIGHT, T. J., ELLIOTT, J. R., WANG, H. & RYDER, I. 2013. Earthquake cycle deformation and the Moho: Implications for the rheology of continental lithosphere. *Tectonophysics,* 609**,** 504-523.

YAMASAKI, T., WRIGHT, T. J. & HOUSEMAN, G. A. 2014. Weak ductile shear zone beneath a major strike-slip fault: Inferences from earthquake cycle model constrained by geodetic observations of the western North Anatolian Fault Zone. *Journal of Geophysical Research: Solid Earth,* 119**,** 3678-3699.